Dalton Transactions

PAPER

View Article Online
View Journal | View Issue

Cite this: *Dalton Trans.*, 2014, **43**, 9924

Structural studies of copper(II) complexes with 2-(2-aminoethyl)pyridine derived Schiff bases and application as precursors of thin organic–inorganic layers†

Magdalena Barwiolek,*[a] Edward Szlyk,[a] Andrzej Berg,[a] Andrzej Wojtczak,[a] Tadeusz Muziol[a] and Julia Jezierska[b]

Received 4th March 2014,
Accepted 29th April 2014

DOI: 10.1039/c4dt00654b

www.rsc.org/dalton

Cu(II) complexes with Schiff bases derived from 2-pyridin-2-ylethanamine were obtained and characterized by UV-Vis, fluorescence, and IR spectra. The X-ray crystal structures determined for [Cu(II)(epy(di-*t*-Buba))Cl] × 0.042H_2O and [Cu(II)(epy(di-*t*-Buba))O_2CCH_3] revealed tetrahedral distortion of the Cu(II) coordination sphere in the solid phase. For both molecules the Cu(II) ions were found in tetragonal environments, as was confirmed by the values of EPR *g*-matrix diagonal components. The thermal properties of the complexes and the gas phase composition were studied by TG/IR techniques. Thin layers of the studied copper(II) complexes were deposited on Si(111) by a spin coating method and characterized by scanning electron microscopy (SEM/EDS), atomic force microscopy (AFM) and fluorescence spectra. For copper(II) layers the most intensive fluorescence band from intra-ligand transition was observed between 498 and 588 nm. The layers' fluorescence intensity was related to the rotation speed and deposition time.

Introduction

Study of copper(II) complexes with Schiff-base ligands has become a point of interest owing to their intriguing structural features and potential application in various fields. These compounds are known for their biological role and fluorescence properties. Schiff base derivatives incorporating a fluorescent moiety are a useful tool for optical sensing of metal ions.[1] Synthesis of Schiff bases and their complexes as fluorescent materials have also received extensive concern.[2]

Pyridine ligands have been used in coordination chemistry for a variety of metals,[3–7] and it has been stated that they play a unique role in synthesis of the biologically active compounds.[8] The fluorescence properties and interaction with DNA of the Schiff bases obtained from imidazole derivatives (*N*-((1*H*-imidazole-2-yl)methyl)-2-(pyridine-2-yl)ethanamine, *N*-((1-methyl-1*H*-imidazole-2-yl)methyl)-2-(pyridine-2-yl)ethanamine; 2-(pyridine-2-yl)-*N*-((pyridine-2-yl)methyl)ethanamine) and their copper(II) complexes were also studied.[9] It has been stated that these complexes effectively interact with CT-DNA through the groove binding mode, resulting in strong conformational changes of the CT-DNA. Copper(II) complexes with imine ligands containing imidazolate bridging groups (*e.g.* *N*,*N*′-bis(2-substituted-imidazol-4-ylmethylidene)-1,4-diaminobutane) have been used as precursors of highly ordered structures.[10–12] Imidazole and oxadiazole-type materials have been used as ETMs in the blue fluorescent OLEDs.[13] As a result, highly efficient amplified spontaneous emission as well as blue and white organic light-emitting diodes (OLEDs) were demonstrated with these imidazole derivatives. As a result, highly efficient amplified spontaneous emission as well as blue and white organic light-emitting diodes (OLEDs) could be demonstrated with these imidazole derivatives.[14] Thin organic and organometallic films have attracted research interest due to their technologically important optical and electronic properties.[15] These materials exhibit luminescence; they are used as conductors, semi-conductors, organic light emitting diodes (OLED) and drug transporters.[16,17] Also many thin films of metal complexes, such as Zn(II), Pt(II), Cu(II) or Ag(I) with Schiff bases (*e.g.* *N*,*N*′-bis(salicylidene)-1,2-ethylenediamine, bis(2-(2-hydroxyphenyl)benzothiazole), were synthesised and their luminescence properties have been employed in organic optoelectronics.[18–22] Some of those films were spin coated or vacuum deposited (4,4′-bis(9-carbazolyl)biphenyl and 2(4-biphenyl)-5-(4-*tert*-butylphenyl)-1,3,4-oxadiazole).[23] However,

[a]*Chemistry Department, Nicholas Copernicus University, 87-100 Torun, Poland. E-mail: madzia@chem.umk.pl, mbarwiolek@umk.pl; Fax: +48 (56) 654 24 77; Tel: +48 (56) 611 45 16*

[b]*Faculty of Chemistry, University of Wroclaw, 50-137 Wroclaw, Poland. E-mail: julia.jezierska@chem.uni.wroc.pl; Fax: +48 71 328-23-48; Tel: +48 (71) 3757330*

†CCDC 950557 and 986880. For crystallographic data in CIF or other electronic format see DOI: 10.1039/c4dt00654b

there are only a few reports on copper(II) compound materials. Some of them were obtained by laser ablation, cathodoluminescence or by spin coating.[13,24–27]

The optical and structural properties of the thin copper(II) layers were also studied. In the case of CuPc (Pc – tetra-tricarbethoxyethyl substituted phthalocyanine), the absorption increase was noted at higher copper concentration in the layers.[24]

Thin layers of the copper(II) complexes $[Cu_3(opba)(pmdta)_2](NO_3)_2$ (pmdta = 1,1,4,7,7-pentamethyl-diethylenetriamine, opba = orthophenylenebis(oxamato)) on SiO_2/Si by the spin coating technique were obtained. The materials exhibited results pointing out that spin coating is a promising method for deposition of thin layers of transition metal complexes. The obtained films were thin and homogeneous with small crystallites on the surface.[13] Also the spin coating technique was used for $[(nBu_3P)_3Cu–O_2CCH_2CO_2–Cu(PnBu_3)_3]$ and $[(nBu_3P)_3Cu–O_2C(CH_2)_2CO_2–Cu(PnBu_3)_3]$ on SiO_2/TiN/Cu deposition. The obtained layers were then heated up to 450 °C, resulting in the complexes' layers undergoing CuO decomposition. The CuO layers exhibited some cracks.[28] SEM results of these films showed not completely homogeneous layers and defects. This was explained by the different film thicknesses obtained during the spin coating process, which upon heating produced defects due to unequal evaporation leading to partially cracked copper films. However, these results indicated that the spin coating technique could be used instead of the CVD method for non-volatile compounds to obtain thin metallic materials.

Previously, copper(II) and nickel(II) complexes with optically active Schiff bases derived from (1*R*,2*R*)(–)cyclohexanediamine were deposited by us on silicon or glass using the spin coating method.[29,30] The obtained materials exhibited luminescence, which depends on the spin coating parameters and the structure of the complex.

The facts mentioned above: the fluorescence properties of the pyridine derivatives and their complexes, the possibility of using the spin coating technique for deposition of the copper(II) complexes on different substrates and the likely fluorescence behaviour of the obtained layers prompted us to synthesize a series of copper(II) complexes with new Schiff bases derived from 2-(2-aminoethyl)pyridine and several aldehydes. These complexes were characterized by X-ray crystallography and spectroscopically, their fluorescence properties were also studied. The new copper(II) complexes were used as precursors of thin layers in the spin coating technique. The morphology of layers was analyzed by AFM and SEM microscopy, and the fluorescence properties of the layers were also studied.

Experimental

Materials

2-Pyridin-2-ylethanamine (epy) (95%), 3,5-di-*tert*-butyl-4-hydroxybenzaldehyde (di-*t*-Buba) (99%), pyridine-2-carbaldehyde (pyca) (99%), 1*H*-imidazole-5-carbaldehyde (4Him) (98%), and pentane-2,4-dione (acacH) (97%) were purchased from Aldrich. Copper(II) chloride dihydrate and copper(II) acetate hydrate (analytical grade) were supplied by POCH (Gliwice Poland) and used as received.

Methods and instrumentation

UV-Vis absorption spectra were recorded on a Milton Roy Spectronic 1201 in CH_3CN (1×10^{-5} M) solution and with a Specord M-40 (Carl Zeiss Jena) spectrophotometer as Nujol mulls. IR spectral experiments were performed on a Spectrum 2000 Perkin/Elmer FT IR using KBr discs in the range 400–4000 cm^{-1} and PE discs in the range 400–70 cm^{-1}. ^1H, ^{13}C, ^{15}N NMR spectra of ligand were collected with a Bruker 400 MHz in $CDCl_3$, against the TMS standard. Elemental analysis of C, H and N was performed on a Vario Macro CHN analyser (Elementar Analysensysteme GmbH), whereas copper elemental analysis was carried by Atomic Absorption Spectroscopy (AAS) as Cu^{2+} salt on an atomic absorption spectrometer (Carl Zeiss-Jena). Thermal analysis (TG, DTG, DTA) was performed on an SDT 2960 TA analyzer at nitrogen flow 60 ml min^{-1}, heating rate 5 °C min^{-1} and heating range up to 1200 °C. Gaseous products of thermal decomposition were detected by a FT IR Bio-Rad Excalibur spectrophotometer equipped with a thermal connector heated to 200 °C for gases evolved from an SDT 2960 TA analyser. Powder X-ray diffraction data for the thermal analysis residues were obtained with a Philips X'PERT diffractometer using Cu Kα radiation.

The EPR spectra were measured using a Bruker ELEXYS E500 spectrometer equipped with an NMR teslameter (ER 036TM) and a frequency counter (E 41 FC) at X- and Q-band. The experimental spectra were simulated using the program Dublet ($S = 1/2$) written by Dr Ozarowski from NHMFL, University of Florida, with resonance field calculated by full diagonalization of the energy matrix.

The films were deposited by the spin coating technique on Si(111) wafers (10\10 mm), glass and ITO. Precursors were dissolved in tetrahydrofuran and deposited on Si using a spin coater (Laurell 650SZ). The morphology and composition of the obtained layers were analyzed with a scanning electron microscope (SEM; LEO Electron Microscopy Ltd, England, model 1430 VP) equipped with detectors of secondary electrons (SE), and an energy dispersive X-ray spectrometer (EDS; Quantax) with an XFlash 4010 detector (Bruker AXS microanalysis GmbH). The atomic force microscopy (AFM) studies in the tapping mode were performed on a Veeco (Digital Instrument) microscope (type: MultiMode NanoScope IIIa). The fluorescence spectra were recorded on an F-7000 spectrofluorometer (HITACHI) in the range 900–180 nm (5×10^{-4} mol dm^{-3} MeCN solution).

X-ray crystallography

The X-ray diffraction data of [Cu(II)(epy(di-*t*-Buba))Cl] × $0.042H_2O$ (**1a**) and of [Cu(II)(epy(di-*t*-Buba))O_2CCH_3] (**1b**) were collected at room temperature using an Oxford Sapphire CCD diffractometer, Mo Kα radiation $\lambda = 0.71073$ Å. The reflections were measured with the ω-2θ method and the analytical

Table 1 Crystal data and structure refinement for [Cu(II)(epy(di-*t*-Buba))Cl] × 0.042H_2O (**1a**) and [Cu(II)(epy(di-*t*-Buba))O_2CCH_3] (**1b**)

Identification code	(**1a**)	(**1b**)
Empirical formula	$C_{22}H_{29.08}ClCuN_2O_{1.04}$	$C_{24}H_{32}CuN_2O_3$
Formula weight	437.21	460.06
Temperature [K]	293(2)	293(2)
Wavelength [Å]	0.71073	0.71073
Crystal system, space group	Trigonal, $R\bar{3}$	Monoclinic, $P2_1/c$
Unit cell dimensions [Å] and [°]	$a = b = c = 15.8718(2)$ $\alpha = \beta = \gamma = 106.6390(10)$	$a = 17.296(2)$ $b = 11.9783(9)$ $c = 12.1930(11)$ $\beta = 105.196(12)$
Volume [$Å^3$]	3362.10(7)	2437.8(4)
Z, Calculated density [Mg m^{-3}]	6, 1.296	4, 1.253
Absorption coefficient [mm^{-1}]	1.107	0.921
F(000)	1377	972
Crystal size [mm]	0.63 × 0.49 × 0.18	0.36 × 0.34 × 0.05
Theta range for data collection [°]	2.45 to 27.09	2.09 to 28.16
Limiting indices	$-20 \le h \le 10$ $-20 \le k \le 20$ $-18 \le l \le 20$	$-21 \le h \le 20$ $-15 \le k \le 13$ $-10 \le l \le 16$
Reflections collected/unique	22 072/4873 [R(int) = 0.0839]	16 433/5400 [R(int) = 0.0812]
Completeness to theta [%]	26.00° [99.9%]	25° [100.0%]
Max. and min. transmission	0.8256 and 0.5423	0.9577 and 0.7354
Data/restraints/parameters	4873/0/250	5400/0/298
Goodness-of-fit on F^2	0.9671.000	0.863
Final R indices [$I > 2$sigma(I)]	$R_1 = 0.0368$, w$R_2 = 0.0956$	$R_1 = 0.0527$, w$R_2 = 0.1065$
R indices (all data)	$R_1 = 0.0518$, w$R_2 = 0.0990$	$R_1 = 0.1424$, w$R_2 = 0.1293$
Largest diff. peak and hole [e $Å^{-3}$]	0.364 and −0.228	0.549 and −0.518

absorption correction was applied for the studied crystals (RED171 package of programs, Oxford Diffraction, 2000[31]). Both structures were solved by direct methods and refined with the full-matrix least-squares procedure on F^2 (package SHELX-97[32]). All heavy atoms were refined with anisotropic thermal displacement parameters. Hydrogen atoms were located from the electron density maps and their positions were constrained in the refinement. In (**1a**) the disordered water molecule is found on the C_{3i} axis and its total occupancy is 0.25. However, this molecule was unstable during the refinement and the thermal parameter was high. Therefore we modelled the solvent disorder in SQUEEZY[33] and subsequently the refinement in SHELXL-97 was repeated resulting in slightly better R factors and a smooth difference electron density map. For (**1b**) the geometric restraints have been used to ensure the proper geometry of the disordered ^{t}Bu group. All figures were prepared in DIAMOND[34] and ORTEP-3.[35] The results of the data collections and refinement are listed in Table 1. The CCDC 950557 and 986880 entries contain the crystallographic data for (**1a**) and (**1b**), respectively.

Synthesis

Synthesis of ligands. Ligands (**1–4**) were prepared by a procedure described in detail for (**1**) and their structural formulae are presented in Fig. 1.

pen(di-*t*-Buba) (**1**) Schiff base was prepared in the reaction of 2-hydroxy-3,5-di-*tert*-butyl-benzaldehyde (2.34 g; 10 mmol in 15 ml MeOH) with 2-(2-aminoethyl)pyridine (1.19 ml; 10 mmol). The mixture was stirred at r.t. for 5 h and the solvent was removed on a rotary evaporator. The product was dried under air. Yield 3.10 g (92.1%).

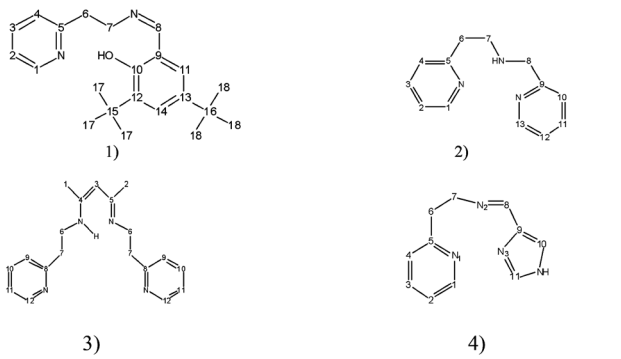

Fig. 1 Structural formula and atom numbering referring to the NMR signals for epy(di-*t*-Buba) (**1**) (*Z*)-2,4-di-*tert*-butyl-6-((2-(pyridin-2-yl)-ethylimino)methyl)phenol, epy(pyca) (**2**) 2-(4,5-dihydropyridin-2-yl)-*N*-(pyridin-2-ylmethyl)ethanamine, (epy)$_2$acacH (**3**) (2*Z*,4*E*)-*N*-(2-(pyridin-2-yl)ethyl)-4-(2-(pyridin-2-yl)ethylimino)pent-2-en-2-amine, epy(4Him) (**4**) (*E*)-*N*-((1*H*-imidazol-4-yl)methylene)-2-(pyridin-2-yl)ethanamine.

^{1}H [ppm]: 1.32 (s, 9H) CH_3, 1.46 (s, 9H) CH_3, 3.21 (t, 2H) CH_2–, 4.02 (t, 2H) CH_2, 7.045 (d 1H), 7.13–7.21 (m, 2H) Ar–H; 7.28 (s, 1H), 7.38 (d, 1H), 7.59–7.63 (m, 1H) Ar–H; 8.58–8.59 (m, 1H) Ar–H; 8.34 (s, 1H) –N═CH–; 13.76 (s, 1H) –OH.[36]

^{13}C [ppm]: 29.42 (C6), 31.5 (C7), 34.1 (C17), 35.03 (C18), 117.83 (C15), 121.47 (C2), 123.70 (C4), 125.83 (C14), 126.83 (C3), 136.43 (C11), 136.63 (C12), 139.93 (C13), 149.45 (C1), 158.10 (C5), 159.27 (C10), 166.39 (C8).

UV-Vis 209 nm π→ π*, 261 nm π→ π*, 329 nm π→ $\pi^*_{N=C}$, 409 nm n→π*.[37–40]

epy(pyca) (**2**) ^{1}H [ppm]: 2.24 (s, 1H); 3.07 (m, 2H), 3.96 (s, 1H), 7.15 (m, 1H); 7.20 (d, 1H), 7.62 (m, 1H); 8.54 (m, 1H), 8.34 (s, 1H) –N═CH–;[36,41]

^{13}C [ppm]: 38.58 (C7), 49.01 (C6), 121.24 (C10), 121.88 (C2), 122.21 (C4), 123.29 (C12), 136.35 (C3), 136.43 (C11), 149.25 (C1), 149.31 (C13), 159.81 (C9), 160.21 (C5), 55.14 (C8).

^{15}N NMR [ppm]: −69.90 (–N═C), −342.47 (NH).

UV-Vis: 211 nm π→ π*, 256 nm π→ π*, 324 nm π→ $\pi^*_{N=C}$, 400 nm n→π*.[37–40]

(epy)$_2$acacH (**3**) ^{1}H NMR [ppm]: 1.85 –CH$_3$ (s, 3H), 1.98 CH$_3$ (s, 3H), 3.04 (t, 4H), CH$_2$–Ar, 3.67 (q, 4H), CH$_2$–N, 4.92 (s, 1H), C═CH–C, 7.09–7.19 (4H), 7.62 (t, 2H), ArH, 8.55 (d, 2H), ArH, 10.90 (br s, 1H), NH–.[36]

^{13}C NMR [ppm]: 18.76 (C1), 28.77 (C2), 38.83 (C6), 42.73 (C7), 95.33 (C3), 121.75 (C11), 123.73 (C9), 136.60 (C10), 149.60 (C12), 158.25 (C8), 162.97 (C4), 194.86 (C5). Fig. 1.

^{15}N NMR [ppm]: N(3) –N═C amine −266.3, −355.9 N(2) NH equals N(1) N═C, −68.7.[42]

UV-Vis: 262 nm π→ π*, 307 nm π→ π*, 311 nm π→ $\pi^*_{N=C}$, 410 nm n→π*.[37–40]

The presence of signals at the ^{1}H, ^{13}C and ^{15}N spectra of (**3**) confirm the tautomeric structure of the isolated compound (**3**).[42–44]

epy(4Him) (**4**) ^{1}H NMR [ppm]: 3.11 (t, 2H) –CH$_2$–N═, 3.42 (s, 1H) –NH–, 3.92 (t, 2H) –CH$_2$–Ar, 7.08–8.48 (m, 6H) CH$_{Ar}$, 9.78 ppm (s, 1H) –N═CH–.[36]

^{13}C NMR [ppm]: 39.4 (C6), 60.5 (C7), 119.8 (C10), 121.6 (C2), 122.3 (C9), 123.7 (C4), 136.6 (C3), 137.7 (C11), 149.1 (C1), 152.6 (C8), 159.3 (C5).

UV-Vis: 257 nm π→ π*, 341 nm π→ $\pi^*_{N=C}$, 406 nm n→π*.[37–40]

Synthesis of complexes

*[Cu(II)(epy(di-t-Buba))Cl] (**1a**).* Copper(II) chloride dihydrate (1.70 g; 10 mmol) in EtOH (10 ml) was added to an ethanolic solution (10 ml) of the ligand (**1**) (3.39 g; 10 mmol). The mixture was stirred for 4 h at r.t. Dark green crystals suitable for X-ray diffraction from C_2H_5OH–C_6H_6 were isolated. Yield: 3.600 g (79.3%), $C_{22}H_{29.08}ClCuN_2O_{1.04}$ (calc./found %): Cu 14.55/14.20, C 60.53/60.81, N 6.41/6.34, H 6.69/7.08.

UV-Vis: 255 nm IL, 285 nm LMCT, 348 nm LMCT, 406 nm LMCT.[37–40]

*[Cu(II)(epy(di-t-Buba))O$_2$CCH$_3$] (**1b**).* The compound was prepared in a similar way as (**1a**) using copper(II) acetate hydrate (1.990 g, 10 mmol). Dark green single crystals of (**1b**) suitable for X-ray analysis were obtained from CH_3Cl–C_6H_6 solution. Yield: 3.340 g (72.7%). $C_{24}H_{32}CuN_2O_3$, calc./found %: Cu 13.81/13.55, C 62.65/62.30, N 6.08/6.23, H 7.01/6.78.

UV-Vis: 238 nm LMCT, 308 nm LMCT, 390 nm LMCT.[37–40]

Complexes (**2a**), (**3a**), (**4a**) were synthesised in the way described above. Results of C, H, and N analysis are as follows: [Cu(II)(epy(pyca))Cl$_2$] (**2a**) Yield: 80.6%. $C_{13}H_{13}CuN_3Cl_2$ calc./found %: Cu 18.38/18.27, C 45.36/45.71, N 12.15/12.11, H 3.79/3.99.

UV-Vis: 202 nm IL, 260 nm IL, 309 nm LMCT.[37–40]

[Cu(II)((epy)$_2$acacH))O$_2$CCH$_3$] (**3a**) Yield: 82.7%. $C_{21}H_{25}CuN_4O_2$ calc./found %: Cu 14.81/14.97, C 58.79/58.46, N 13.06/12.95, H 5.87/5.84.

UV-Vis: 205 nm IL, 254 nm IL, 316 nm LMCT.[37–40]

[Cu(II)(epy(4Him))O$_2$CCH$_3$] (**4a**) Yield: 68.2%. $C_{13}H_{15}CuN_4O_2$ calc./found %: Cu 19.86/19.40, C 48.82/49.19, N 17.52/17.42, H 4.68/4.24.

UV-Vis: 205 nm IL, 258 nm IL, 313 nm LMCT.[37–40]

Results and discussion

Structure of [Cu(II)(epy(di-*t*-Buba))Cl] × 0.042H$_2$O (1a)

The [Cu(II)(epy(di-*t*-Buba))Cl] × 0.042H$_2$O (**1a**) crystallized in the rhombohedral $R\bar{3}$ space group with the whole molecule in the asymmetric unit. However, the disordered and relatively poorly refined water molecule is excluded from the final model as was mentioned in the Experimental part. The copper(II) coordination sphere is composed of two nitrogen atoms and one oxygen from the Schiff base and chloride (Fig. 2). It adopts the strongly distorted square planar environment with angles in two ranges from 145.23(8) (O1–Cu1–N17) to 150.98(5) (N9–Cu1–Cl2) and from 93.12(7) (N9–Cu1–N17) to 96.03(5)° (N17–Cu1–Cl2). In the coordination sphere, the pyridine nitrogen occupies the *cis* position relative to N9 and Cl atoms. The O1 (phenol) atom is *trans* to the N17 (pyridine) atom, whereas the aliphatic N9 (azomethine) atom is *trans* to chloride. All Cu–X (X = N, O, Cl) bonds differ significantly with the shortest values observed for the Cu–O1 (phenol) bond (1.8724(15) Å) and the biggest ones for Cu–Cl (2.2187(6) Å). The Cu–N$_{(aryl)}$ is much longer (by approximately 0.05 Å) than N$_{(alkyl)}$. The phenyl and pyridyl rings remain flat with an r.m.s. of 0.006 Å. Two chelate rings differ significantly in their conformation: the Cu1–O1–C2–C7–C8–N9 ring is flat with an r.m.s. of 0.016 Å, whereas the Cu1–N17–C12–C11–C10–N9 ring is strongly folded with an r.m.s. of 0.296 Å and the largest deviation of 0.493(2) Å observed for C11.

The phenyl and pyridine ring systems form a dihedral angle of 49.34(13)°. The phenyl and Cu1–O1–C2–C7–C8–N9 chelate rings are coplanar with an angle of 2.57(9)°, whereas Cu1–N17–C12–C11–C10–N9 chelate and pyridine rings are inclined by 27.54(12)°. Both chelate rings form an angle of 21.62(9)°. Hence, the Schiff base exhibits a bowl shape with the copper(II) ion on its top and shows a shift by 0.51 Å from the plane defined by the coordinating O1, N9 and N17 atoms. Such an

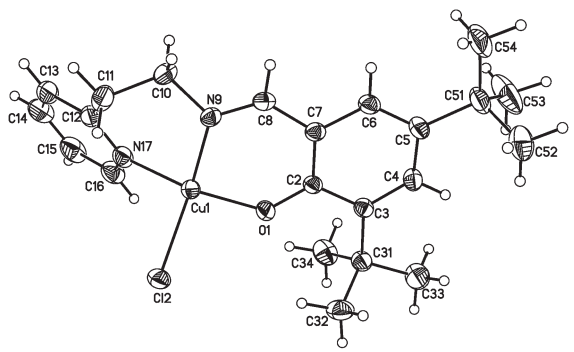

Fig. 2 Molecule of [Cu(II)(epy(di-*t*-Buba))Cl] × 0.042H$_2$O (**1a**) with the numbering scheme and thermal ellipsoids at 30% probability.

orientation of aromatic rings is assured by conformation of the –CH═N–CH_2–CH_2– linker and the most important impact reveals dihedral angles around C10–C11 and C11–C12 bonds from the folded N17 chelate rings showing values of −62.1(3) and 61.4(3)°, respectively. The geometry of the Schiff base motif is described by a C8–N9 distance of 1.283(3) and C7–C8–N9 and C8–N9–C10 angles of 128.03(19) and 115.66(17)°, respectively. The C2–C7–C8–C9 torsion angle describing the geometry of the O1 chelate ring is −0.7(3)° indicating that this ring is flat as was shown also by r.m.s. deviation.

The structure of **1a** reveals the porous nature with channels running along the *c*-axis filled with water molecules. Every channel is encompassed by six adjacent channels. They are surrounded by six complex molecules arranged in two inverted triangles forming the ···–AB–AB–··· pattern of layers. The dash indicates large separation between triangles. It can be estimated as Cu–Cu distance being 6.551 Å inside –AB– and 15.249 Å between B–A pairs of triangles. In the former case six molecules form a single pore. The diameter of these channels is approximately 5.2 Å. Hence, the water molecule located in this position could not interact with walls of the pore and should be easily removed. Therefore, it was unstable in the refinement and revealed a high thermal parameter. Six molecules forming walls of the pore coming from –AB– layers are connected due to C10–H10···Cl2 ($-z$, $1-x$, $1-y$) hydrogen bonds. Additionally, there are numerous π–π interactions, mainly between strongly inclined rings of the molecules forming the pore and C15–H15···π interactions with the O1 chelate ring. Interactions between adjacent –AB– modules in the channel, translated along the *c*-axis, do not exist due to significant separations between molecules. However, there are interactions between adjacent modules from different channels. They concern two closest copper(II) ions separated by 5.078 Å and are formed due to C11–H11···π interactions with the phenyl ring and numerous π–π interactions, including stacking interactions between close, well-oriented and revealing small slippage two O1 chelate rings (Table 2).

Table 2 Selected interactions bond lengths [Å] and angles [°] for [Cu(II)-(epy(di-*t*-Buba))Cl] (**1a**)

Bonds			
Cu1–O1	1.8724(15)	Cu1–N17	1.9892(19)
Cu1–N9	1.9351(17)	Cu1–Cl2	2.2187(6)
Angles			
O1–Cu1–N17	145.23(8)	N9–Cu1–Cl2	150.98(5)
N9–Cu1–N17	93.12(7)	N17–Cu1–Cl2	96.03(5)
O1–Cu1–N9	94.16(6)	O1–Cu1–Cl2	93.85(5)

X-ray crystal structure of [Cu(II)(epy(di-*t*-Buba))O_2CCH_3] (1b)

In (**1b**), the Cu(II) ion is coordinated by the asymmetric Schiff base and the acetate ligand (Fig. 4) resulting in CuN_2O_3 square pyramidal geometry. Among the equatorial bonds, the Cu1–O1 (phenolate) distance of 1.878(3) Å is much shorter than that for Cu1–O2 (acetate) of 1.960(2) Å. There is a significant difference between Cu1–N1 (benzaldehyde) 1.937(3) and Cu1–N2

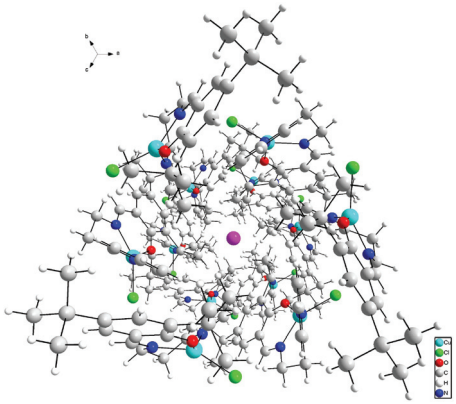

Fig. 3 Perspective view of (**1a**) along the [111] direction revealing channels of 5.2 Å diameter filled with partially occupied water molecules.

(pyridine) 1.989(3) Å, which is similar to that found in (**1a**). The axial bond Cu1–O3 of 2.517(3) Å is formed by the acetate oxygen. Different C23–O bond lengths for the carboxylate anion (Table 3) were noted, indicating that O2 is a carboxylate atom, while O3 forms a double bond to C23.

The CuN_2O_2 equatorial plane exhibits a significant tetrahedral deformation with the atom displacement from the best plane ranging from O1 0.440(2) Å to O2 −0.399(1) Å. Atoms N1 and O2 are displaced from the CuN_2O_2 plane towards axial O3, while O1 and N2 are displaced in an opposite direction. A similar geometry of the square-planar coordination sphere was reported for [{(2-etpy(sal))Cu}{μ-[Ag(CN)$_2$]}] and [{(2-etpy(sal))-Cu}{μ-[Cu(CN)$_2$]}] complexes.[45] In the equatorial plane, the pairs of atoms positioned *trans* define N1–Cu1–O2 and O1–Cu1–N2 angles of 159.90(11) and 151.58(11)°, respectively, values larger than those reported for (**1a**). The angles formed by the atoms in the *cis* positions range from 90.10(11) to 94.87(14) and are significantly smaller than those found in (**1a**). That seems to reflect the difference caused by the bulk of chloride ligand in (**1a**). The angles between equatorial bonds formed by O1, N1 and N2 and axial Cu1–O3 are 97.44(11), 103.36(10) and 107.25(10)°, respectively. The O2–Cu1–O3 angle involving both oxygen atoms of the acetate ligand equals is 56.54(9)°.

The dihedral angle between the phenolate and pyridyl rings of the Schiff base ligand is 13.6(2)° and is much smaller than that reported for (**1a**). Such a flat environment may be coupled to the position of the acetate ligand, almost perpendicular to the plane defined by both these rings, with the dihedral angles between phenolate and pyridyl rings and the plane Cu1–O2–C23–O3 being 79.46(12) and 76.54(10)°, respectively. The torsion angle Cu1–O2–C23–O3 describing the rotation of acetate around the coordination Cu1–O2 bond is 8.2(5)°. The acetate ligand is slightly tilted relative to the equatorial CuN_2O_2 plane, with the dihedral angle between these planes being 80.41(15)°.

The valence geometry of the Schiff base ligands is typical for such systems. The C7–N1 distance is 1.280(5) Å, C6–C7–N1 and C7–N1–C8 angles are 127.0(4) and 117.8(3)°, respectively, and are similar to those observed in (**1a**). The phenolate-Schiff base moiety of the ligand is almost flat, with the torsion angles C1–C6–C7–N1 and C6–C7–N1–C8 being 8.9(6)° and

Table 3 Selected bond lengths [Å] and angles [°] for [Cu(II)(epy(di-*t*-Buba))O_2CCH_3] (**1b**)

Cu1–O1	1.878(3)
Cu1–N1	1.937(3)
Cu1–O2	1.960(2)
Cu1–N2	1.989(3)
Cu1–O3	2.517(3)
O1–Cu1–N1	92.84(13)
O1–Cu1–O2	90.10(11)
N1–Cu1–O2	159.90(11)
O1–Cu1–N2	151.58(11)
N1–Cu1–N2	94.87(14)
O2–Cu1–N2	91.92(11)
O3–Cu1–O1	97.44(11)
O3–Cu1–O2	56.54(9)
O3–Cu1–N1	103.36(10)
O3–Cu1–N2	107.25(10)
C1–O1–Cu1	126.5(2)
C7–N1–Cu1	121.9(3)
C8–N1–Cu1	119.8(3)
C10–N2–Cu1	122.8(3)
C14–N2–Cu1	118.6(3)
C23–O2–Cu1	102.7(2)

−178.0(3)°. However, the ethylaminepyridil fragment is significantly folded with consecutive torsion angles C7–N1–C8–C9, N1–C8–C9–C10 and C8–C9–C10–N2 being −140.6(3), −72.8(5) and 54.9(5)°. The C19 ^{t}Bu group reveals a rotational disorder with two equally populated rotamers (50/50%).

The six-membered chelate rings Cu1–O1–C1–C6–C7–N1 and Cu1–N1–C8–C9–C10–N2 are an envelope on Cu1 and a boat, respectively. In the four-membered ring Cu1–O2–C23–O3 the torsion angles have alternating negative and positive values ranging from −6.4(4) to 8.2(5)°.

Analysis of crystal packing revealed the π–π interaction between the C1–C6 phenyl ring and pyridine C10–N2[1 − *x*, −*y*, −*z*] with the angle between two rings of 13.57° and the distance between their gravity centers Cg–Cg of 3.885(3) Å. There is an intermolecular C7–H7A...O3[*x*, −1/2 − *y*, −1/2 + *z*] interaction involving the Schiff base C–H and acetate oxygen, with the C···O distance of 3.398(4) Å (Fig. 5). Two methyl groups of C15 ^{t}Bu are involved in the intramolecular interactions C16–H16C...O1 and C17–H17B...O1, with C···O distances being 2.958(6) and 2.958(7) Å, respectively.

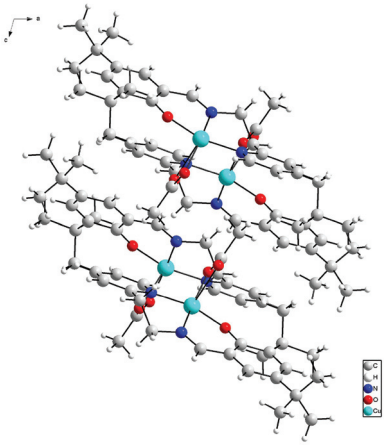

Fig. 5 Packing of (**1b**) viewed along the *c*-axis.

Both reported structures have different counterions that heavily influence the packing and absorption properties. Only the (**1a**) structure is porous (Fig. 3). Moreover, at the molecular level the counterions affect the coordination number. In (**1a**), the coordination sphere adopts a strongly distorted square planar environment, whereas in (**1b**) it is a strongly elongated tetragonal pyramid. In both cases the valence geometry of the Schiff base is similar. However, some conformational differences are detected, of which the most important occurs for the C8–N9–C10–C11 angle, being −171.98(19)° in (**1a**) and −140.6(3)° in (**1b**) structure.

EPR analysis. The EPR spectra at the Q-band of polycrystalline compounds [Cu(II)(epy(di-*t*-Buba))Cl] (**1a**) and [Cu(II)(epy-(di-*t*-Buba))O_2CCH_3] (**1b**) exhibit a much better resolution of two signals for (**1a**) and three signals for (**1b**) (Table 4) than those measured at X-band (Fig. 6). Although the EPR spectra could be treated as showing axial and orthorhombic symmetry of the Cu(II) centers, respectively, the values of g_1 parameters are too small considering: (a) a type of donors coordinated in the Cu(II) plane, (NON)Cl and (NON)O, and (b) a significant deviation of planar to tetrahedral geometry, which imposes the increase of *g*-matrix diagonal components.[46]

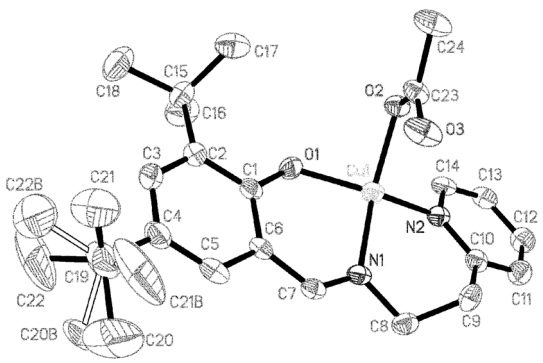

Fig. 4 Molecule of [Cu(II)(epy(di-*t*-Buba))O_2CCH_3] (**1b**) with the numbering scheme and thermal ellipsoids at 30% probability. For clarity, H atoms for the disordered ^{t}Bu were omitted.

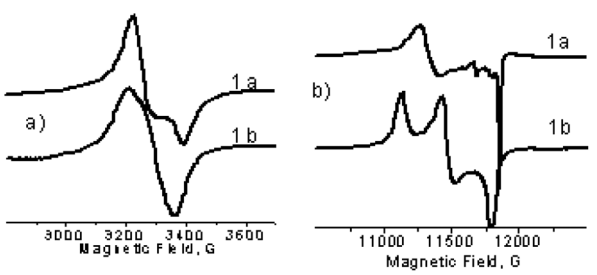

Fig. 6 EPR of polycrystalline compounds (**1a**) and (**1b**) (a) at X-band (about 9.7 GHz) at room temperature and (b) at Q-band (about 36 GHz) at room temperature. The weak signals for (**1b**) in the middle of the spectrum at the Q-band correspond to the resonance transitions due to differently oriented crystallites.

Table 4 EPR spectra of coupled and molecular *g*-matrix parameters and crystal structure data for (**1a**) and (**1b**)

			c	g_{av}	Cu–Cu [Å]	Canting angle [°]	
Cu(salgly)diPhTu × H_2O	g_1^c = 2.145 g_z = 2.228[a]	g_2^c = 2.145 g_y = ~2.065[a]	g_3^c = 2.042 g_x = ~2.04[a]	2.111 2.111		90[a]	47
Cu(salval)P × P	g_1^c = 2.179 g_z = 2.247[a]	g_2^c = 2.127 g_y = 2.066[a]	g_3^c = 2.050 g_x = 2.045[a]	2.119 2.119	6.131	74.0	48
[Cu(II)(epy(di-*t*-Buba))Cl] (**1a**)	g_1^c = 2.146	g_2^c = 2.146	g_3^c = 2.047	2.113	6.550	60.41	This work
[Cu(II)(epy(di-*t*-Buba))O_2CCH_3] (**1b**)	g_1^c = 2.180	g_2^c = 2.115	g_3 = 2.059	2.118	6.352	76.23	This work

[a] Calculated on the basis of EPR data.

Hence, the spectra can be considered to be a result of co-operative effects due to the magnetic exchange between the non-equivalent paramagnetic centers. The observed values of the *g* components are caused by the coupling of *g* matrixes giving g_1^c, g_2^c and g_3^c parameters (Table 4). The crystal structure reveals that for [Cu(II)(epy(di-*t*-Buba))Cl] (**1a**) the interactions may arise at the shortest Cu···Cu distance of 6.550 Å for non-parallel coordination polyhedra, whose planes Cl2–O1–N17–N9 are canted by 60.41°. The monomeric units are joined by C10–H10···Cl2 interactions and numerous π–π interactions, mainly between strongly inclined rings of the molecules. For [Cu(II)-(epy(di-*t*-Buba))O_2CCH_3] (**1b**) the dihedral angle between Cu1–O2–O1–N1–N2 planes is 76.23° for the Cu(II) centers separated by 6.352 Å. There are also intermolecular C7–H7A···O3 interactions involving the Schiff base C–H and acetate oxygen as well as π–π interactions between inclined phenyl and pyridine rings.

The Q-band spectra of [Cu(II)(epy(di-*t*-Buba))Cl] (**1a**) and [Cu(II)(epy(di-*t*-Buba))O_2CCH_3] (**1b**) are similar to those reported[47,48] for Cu(II) complexes with tridentate ONO Schiff bases and monodentate X ligands, Cu(salgly)diPhTuxH_2O where salgly = *N*-salicylidene-glycine and diPhTu = *N*,*N*′-diphenylthiourea and Cu(salval)P × P where salval = *N*-salicylidene-(*R*,*S*)-valine, P = pyrazole. The molecular EPR parameters were calculated for those complexes using the approximate relations between the canting angles (the angles formed by the tetragonal axis of magnetically non-equivalent chromophores)[47] and the coupled g_c components. Although the coupled *g* components listed in Table 4 have very close values, the molecular *g* tensor components of individual [Cu(II)(epy(di-*t*-Buba))Cl] (**1a**) and [Cu(II)(epy(di-*t*-Buba))O_2CCH_3] (**1b**) complexes should exhibit stronger rhombicity than the parameters calculated for Cu(II) complexes with ONO Schiff bases. The latter can be caused by significant tetrahedral distortion in the Cu(II) plane in [Cu(II)(epy(di-*t*-Buba))Cl] (**1a**) and [Cu(II)(epy(di-*t*-Buba))-O_2CCH_3] (**1b**). Also a higher value of g_z should be expected, close to 2.26 according to the parameters observed for Cu(II) complexes with different tridentate ONN[49] and ONN[50] Schiff bases and polar solvents.

Infrared spectroscopy

The IR spectra of free ligands exhibit bands from –N=CH– stretching vibrations in the region 1591–1623 cm^{-1}.[37,54] The spectrum of epy(di-*t*-BubaH) (**1**) exhibits the Ph–O stretching vibration band at 1235 cm^{-1}, whereas the –OH stretching vibration band was noted at 3467 cm^{-1}. Upon complexation, the Ph–O stretching vibration band was shifted towards higher frequencies (1256 cm^{-1} for (**1a**) and 1251 cm^{-1} for (**1b**)), while –OH stretching vibration bands have disappeared.[51–53]

Moreover, the band from azomethine stretching vibrations in (**2a**) was noted at 1608 cm^{-1} for [Cu(II)(epy(pyca))Cl_2], $\Delta_{coord} = \Delta_{comp} - \Delta_{lig}$ = 17 cm^{-1} for (**2a**), which confirms the copper binding by the –N=CH– group. Also, the stretching vibrations of –NH– for (**2a**) were observed at 3446 cm^{-1} (Δ = 12 cm^{-1}) for (**2a**), which confirms the coordination *via* the pyridine nitrogen atom. In the spectrum of [Cu(epy(di-*t*-Buba))Cl] × 0.042H_2O (**1a**) at 3436 cm^{-1} a band from stretching vibrations of the –OH group was registered.

In the spectra of [Cu(II)(epy(4Him))O_2CCH_3] (**4a**), (**1b**) and [Cu(II)((epy)$_2$acacH)O_2CCH_3)] (**3a**), the bands from symmetrical and asymmetrical stretching vibrations of the carboxylate group in the region 1403–1474 cm^{-1} $\nu_s COO^-$ and 1628–1742 cm^{-1} $\nu_{as} COO^-$ were registered,[54] suggesting the monodentate coordination.

Moreover, the band from Cu–N vibrations was noted at 428 cm^{-1} (**2a**), whereas the band from Cu–O stretching vibrations was registered at 507cm^{-1} (**4a**), at 543 cm^{-1} (**1a**), at 588 cm^{-1} (**1b**), and at 526 cm^{-1} (**3a**).[55] Additionally, the band from Cu–Cl stretching vibrations appears at: 309 cm^{-1} [Cu(II)-(epy(pyca))Cl_2] (**2a**) and 352 cm^{-1} (**1a**).[54] The presence of the bands from Cu–O, Cu–N and Cu–Cl stretching vibrations confirms the coordination *via* Ph–O, N and Cl atoms respectively.

Summarizing IR results for the studied complexes it is evident that the copper(II) ions coordinate with the ligand *via* N or O atoms and Cl^- or CH_3COO^- ions.

Thermal analysis of the complexes

The DTA curve of [Cu(II)(epy(di-*t*-Buba))Cl] (**1a**) revealed an endothermic process between 38 and 998 °C. Analysis of the DTG curve indicates one process corresponding to the detachment of the organic ligand (TG mass loss 71.24%). The final product of decomposition was CuCl (calc. 16.83%, exp. 16.34%), as was confirmed by the XRD analysis.

The decomposition of [Cu(II)(epy(di-*t*-Buba))O_2CCH_3] (**1b**) is also a one step endothermic process (Fig. 7). On the DTG peak (T_{max} = 266 °C, 77.85% sample mass loss) corresponding to

the Schiff base, detachment was observed. The final product of decomposition was the mixture of CuO with carbon impurities.

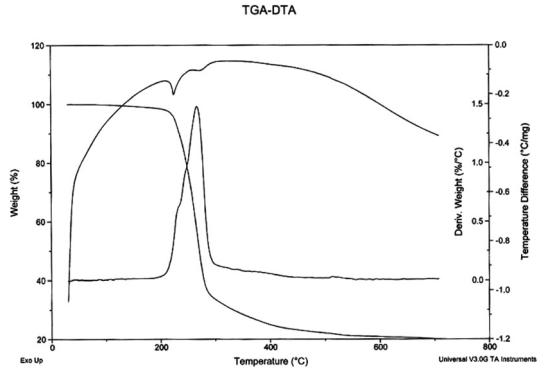

Fig. 7 Thermogram of [Cu(II)(epy(di-*t*-Buba))O_2CCH_3] (**1b**).

The thermal decomposition of the [Cu(II)((epy)$_2$acacH))-O_2CCH_3] (**3a**) is an exothermic process (T_i = 145 °C, T_{max} = 191 °C and T_f = 1190 °C). As for (**1a**) and (**1b**), the final product of decomposition was CuO (mass of residue calc. 18.94%; exp. 18.32%).

In the case of [Cu(II)(epy(pyca))Cl_2] (**2a**) the decomposition is a multistage process (T_i = 26 °C and T_f = 964 °C). On the DTG curve seven exothermic processes with maxima at: 58 °C, 163 °C, 175 °C, 249 °C, 329 °C, 437 °C and 1010 °C were observed, which can be assigned to the detachment of chlorine and partial decomposition of the Schiff base (total mass loss 81.40%). The final product of the decomposition process was metallic Cu (calc. 18.6%, exp. 18.6%).

The thermogram of [Cu(II)(epy(4Him))O_2CCH_3] (**4a**) exhibits four DTG peaks with maxima at 314, 394, 505 and 642 °C, and the TG curve reveals four stages with 3.68, 7.75, 29.27 and 11.30% sample mass loss. The first step with a maximum at 184 °C at the DTA curve can be related to the detachment of the acetic acid molecule (mass loss 18.66%, calc. 18.69%). The assignment was confirmed by the IR spectra of gases evolved during measurement, where the bands at 1394 and 1774 cm^{-1} from $\nu_{COO-sym}$ and $\nu_{COO-asym}$ vibrations were observed.[39] Afterwards the partial dissociation of the Schiff base occurs leaving the metallic copper (the % mass of residue 17.42% calc., exp. 19.78%). In the studied cases, the final product of the thermal decomposition of copper(II) complexes was copper oxide or metallic copper. The [Cu(II)(epy(4imH))O_2CCH_3] (**4a**) complex is thermally more stable than others because it was not completely decomposed below 1200 °C.

Thin layer studies

The copper(II) organic–inorganic layers on a silicon substrate were deposited by the spin coating technique. Because the parameters of the layers depended on the spin speed and time of coating for all experiments, time was set to 30 s and spin speed to 900, 1000, 1100 and 2000 rpm. The layers' morphology was studied by SEM/EDX.

The SEM images revealed that silicon surfaces are uniformly covered by the Cu(II) complex. The layers are amorphous, but sporadically crystalline structures appeared. The calculated dimensions of these crystallites ranged from 0.5 to 2.0 μm. The latter can be caused by non-completed solidification of the complex solution during the spin coating process. The EDS results indicated that the copper contents decrease in the layers obtained at higher rotation speed. The latter corresponds to thinner layer formation upon the increase of the rotation speed. For the majority of complexes, the best coverage and smooth layers were obtained at 1100 rpm and time 30 s. The obtained surfaces, in particular their roughness and thickness, were analyzed by AFM measurements and results are presented in Fig. 8.

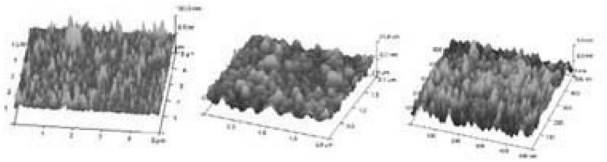

Fig. 8 AFM images of the [Cu(II)(epy(pyca))Cl_2] (**2a**)/Si(111) layers: (a) 900 rpm min^{-1}, (b) (**2a**)/glass 1000 rpm min^{-1}, and (c) (**2a**)/ITO 1000 rpm min^{-1}.

The images in Fig. 8 reveal that the smallest and most uniform particles are on the Si surface, whereas on ITO there are the highest dimensions of the complex particle. On the glass substrate, particles revealed the biggest dissipation of variation in size and did not cover the substrate surface uniformly. The complex [Cu(II)(epy(pyca))Cl_2] (**2a**) forms layers uniformly covering the silicon surfaces at all the used spin speeds. Deposition of compound (**2a**) on the glass slides and ITO was also performed (Fig. 8). The highest value of R_q and R_a (average of image data without application of the surface height deviations measured from the mean plane) parameters were registered for the layers covering the glass slides. These measurements indicated that the type of the substrate also affects the morphology of the obtained layer. In the case of **2a**) the layers deposited on glass are rougher than those obtained on silicon or on ITO substrates. The uniformly covered materials were received at 900, 1000, 2000 rpm min^{-1} spin speed.

In the case of (**1a**)/Si and [Cu(II)(epy(di-*t*-Buba))O_2CCH_3] (**1b**)/Si, homogeneous layers without significant differences in roughness were obtained. The optimal spin speed was 1100 rpm min^{-1} (R_q and R_a parameters equal 35.1 and 24.9 nm for (**1a**)/Si and 103 and 70.1 nm for (**1b**)/Si). For (**1a**)/Si, doubling of the spin speed and repetition of this process (time 10 s) lead to a smoother layer with: R_q = 0.572 nm and R_a = 0.842 nm. The depth of the layer equals 6 nm. For (**4a**)/Si, the optimal spin speed giving a smooth layer with equally spread compounds was 2000 rpm min^{-1} (R_a = 15.3 nm). The content of Cu in this layer equals 3.11%.

The above discussion suggests that the quality of the layer (uniformity, roughness) can be optimized by the variation of spin speed and deposition time. Concluding, the obtained layers are thin and homogeneous with equally spread complexes over the substrate surface.

Fluorescence properties of the layers

The Schiff bases are known for their fluorescence properties and their varied applications.[56] Therefore, we studied the luminescence properties of the obtained compounds and layers.

In the case of (**1a**) and (**1b**), the highest fluorescence band intensities were observed for λ_{ex} = 269 nm and 280 nm for [Cu(II)(epy(di-*t*-Buba))Cl] (**1a**) and [Cu(II)(epy(di-*t*-Buba))-O_2CCH_3] (**1b**) respectively. The emission band from intraligand π*→π transitions was observed at 538 nm for (**1a**) and 560 nm for (**1b**).[37–39] The highest fluorescence intensity of the layers (**1a**)/Si and (**1b**)/Si was noted when the rotation speed was set to 2000 rpm min^{-1}. These layers revealed the best smoothness and uniformity. Besides, EDX results indicated that these layers exhibited the highest content of copper (12.48% for (**1a**) and 6.84% for (**1b**)).

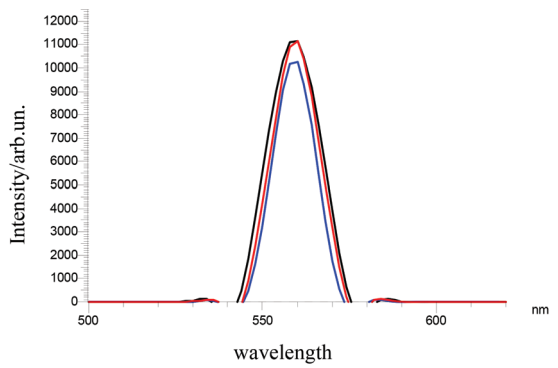

Fig. 9 Fluorescence spectra of [Cu(II)(epy(pyca))Cl_2] (**2a**)/Si, ––– 900 rpm min^{-1}, - - - 1000 rpm min^{-1}, - - - 1100 rpm min^{-1}, λ_{ex} = 280 nm, λ_{em} = 560 nm.

The [Cu(II)(epy(4Him))O_2CCH_3] (**4a**)/Si, [Cu(II)((epy)$_2$acacH)-O_2CCH_3] (**3a**)/Si materials also exhibit fluorescence λ_{em} = 552 and 588 nm (λ_{ex} = 277 (**4a**)/Si and 295 nm (**3a**)/Si). These layers were obtained at 1100 rpm min^{-1} (R_a = 19.7 nm (**4a**)), respectively. Again they revealed the highest content of copper.

When the spin speed was set to 2000 rpm min^{-1}, the highest intensity of the fluorescence (λ_{em} = 560 nm) was observed for (**2a**)/Si material (λ_{ex} = 280 nm) (Fig. 9). However, the hybrid layers of (**2a**) on the glass slides exhibit lower intensity than on the silicon wafers. The optimal spin speed for (**2a**)/ITO was 1000 rpm min^{-1} when the excitation was set at 250 nm and λ_{em} = 498 nm.

Additionally, the copper(II) complex fluorescence spectra were also recorded in MeCN solution. The spectra exhibited emission bands between 365 and 588 nm from the intraligand π*→π transition (λ_{ex} = 277–295 nm). Spectra of complexes registered in solution revealed a much lower intensity of the fluorescence bands than the bands of complex layers.

These studies suggest that better smoothness of layers and higher complex concentration result in higher fluorescence intensity.

Conclusions

The series of Schiff bases and their copper(II) complexes were obtained. The X-ray crystal data for copper(II) complexes indicated that the planar environment strongly distorted towards tetrahedral geometry in the case of the [Cu(II)(epy(di-*t*-Buba))-Cl] × 0.042H_2O (**1a**). This structure reveals porous nature with channels filled with water molecules running along the *c*-axis. In the complex [Cu(II)(epy(di-*t*-Buba))O_2CCH_3] (**1b**), the Cu(II) ion is coordinated in CuN_2O_3 square pyramidal geometry by Schiff base and acetate ligands. The X-ray analysis results suggested a significant influence of the anion on the geometry of the coordination sphere. The EPR studies revealed the cooperative effects due to magnetic interactions between Cu(II) ions forming non-parallel coordination polyhedra. The final products of the thermal decomposition were either copper oxide or metallic copper and even a mixture of the copper oxide with carbon. The thin layers containing copper(II) Schiff base complexes exhibited fluorescence. The highest intensity of the fluorescence was noted for the smooth layers obtained at 1100 rpm min^{-1} or 2000 rpm min^{-1} which revealed the highest copper content. The emission was observed at 490–560 nm and is connected to the intraligand π*→π transitions. The fluorescence emission of the layers makes these materials potentially suitable for application in light emitting devices.

Acknowledgements

Authors would like to thank the National Science Centre (NCN), Poland for financial support (grant no. 2013/09/B/ST5/03509).

References

1 L. N. Wang, W. W. Qin and W. S. Liu, *Inorg. Chem. Commun.*, 2010, **13**, 1122–1125.
2 P. A. Vigato, S. Tamburini and L. Bertolo, *Coord. Chem. Rev.*, 2007, **251**, 1311–1492.
3 M. Shavit and E. Y. Tshuva, *Eur. J. Inorg. Chem.*, 2008, 1467–1474.
4 M. Zhao, B. Helms, E. Slonkina, S. Friedle, D. Lee, J. DuBois, B. Hedman, K. O. Hodgson, J. M. J. Frechet and S. J. Lippard, *J. Am. Chem. Soc.*, 2008, **130**, 4352–4363.
5 L. Dubois, J. Pecaut, M.-F. Charlot, C. Baffert, M.-N. Collomb, A. Deronzier and J.-M. Latour, *Chem. – Eur. J.*, 2008, **14**, 3013–3025.

6 C. I. Yang, W. Wernsdorfer, Y.-J. Tsai, G. Chung, T.-S. Kuo, G.-H. Lee, M. Shieh and H.-L. Tsai, *Inorg. Chem.*, 2008, **47**, 1925–1939.
7 M. Vasconcellos-Dias, C. D. Nunes, P. D. Vaz, P. Ferreira and M. J. Calhorda, *Eur. J. Inorg. Chem.*, 2007, 2917–2925.
8 S. Jong-Keun, Z. Long-Xuan, B. Arjun, T. Pritam, K. Radha, N. Younghwa, J. Yurngdong, J. Tae Cheon, J. Byeong-Seon, L. Chong-Soon and L. Eung-Seok, *Eur. J. Med. Chem.*, 2008, **43**, 675–682.
9 P. Kumar, S. Gorai, M. Kumar Santra, B. Mondal and D. Manna, *Dalton Trans.*, 2012, **41**, 7573–7581.
10 W. A. Alves, G. Cerchiaro, A. Paduan-Filho, D. M. Tomazela, M. N. Eberlin and A. M. Da Costa Ferreira, *Inorg. Chim. Acta*, 2005, **358**, 3581–3591.
11 M. Mimura, T. Matsuo, T. Nakashima and N. Matsumoto, *Inorg. Chem.*, 1998, **37**, 3553–3560.
12 Y. Sunatsuki, Y. Motoda and N. Matsumoto, *Coord. Chem. Rev.*, 2002, **226**, 199–209.
13 M. Szybowicz, T. Runka, M. Drozdowski, W. Bała, A. Grodzicki, P. Piszczek and A. Bratkowski, *J. Mol. Struct.*, 2004, **704**, 107–113.
14 S. Park, J. S. Seo and S. Y. Park, *Adv. Funct. Mater.*, 2012, **14**, 8878–8884.
15 C. H. Chen and J. Shi, *Coord. Chem. Rev.*, 1998, **171**, 161–174.
16 C. Sanchez, L. Rozes, F. Ribot, C. Laberty-Robert, D. Grosso, C. Sassoye, C. Boissiere and L. Nicole, *C. R. Chim.*, 2010, **13**, 3–39.
17 B. Brauer, D. R. T. Zahn, T. Ruffer and G. Salvan, *Chem. Phys. Lett.*, 2006, **432**, 226–229.
18 C. M. Che, S. C. Chan, H. F. Xiang, M. C. W. Chan, Y. Liu and Y. Wang, *Chem. Commun.*, 2004, 1484–1485.
19 T. Sano, Y. Nishio, Y. Hamada, H. Takahashi, T. Usuki and K. Shibata, *J. Mater. Chem.*, 2000, **10**, 157–161.
20 K. H. Chang, C. C. Huang, Y. H. Liu, Y. H. Hu, P. T. Chou and Y. C. Lin, *J. Chem. Soc., Dalton Trans.*, 2004, 1731–1738.
21 R. Ghosh, Sk. H. Rahaman, C. N. Lin, T. H. Lu and B. K. Ghosh, *Polyhedron*, 2006, **25**(16), 3104–3112.
22 Y. Hu, X. Gao, C. Di, X. di Yang, F. Zhang, Y. Liu, H. Li and D. Zhu, *Chem. Mater.*, 2011, **23**(5), 1204–1215.
23 S. Park, J. Seo, S. H. Kim and S. Y. Park, *Adv. Funct. Mater.*, 2008, **18**, 726–731.
24 I. Sorar, M. K. Şener, F. Z. Tepehan, A. Gül and M. B. Koçak, *Thin Solid Films*, 2008, **516**, 2894–2898.
25 W. Ting-ting, He Zhi-qun, Z. Xiao-pan, W. Yong-sheng, Z. Chun-xiu and Z. Wen-guan, *Optoelectron. Lett.*, 2007, **3**(1), 43–46.
26 W. Qiu, W. Hu, Y. Liu, S. Zhou, Yu Xu and D. Zhou, *Sens. Actuators, B*, 2001, **75**, 62–66.
27 P. M. Sirimanne, M. Rusop, T. Shirata, T. Soga and T. Jimbo, *Mater. Chem. Phys.*, 2003, **80**, 461–465.
28 A. Jakob, T. Rüffer, P. Djiele, P. Ecorchard, B. Walfort, K. Körbitz, S. Frühauf, S. E. Schulz, T. Gessner and H. Lang, *Z. Anorg. Allg. Chem.*, 2010, **636**, 1931–1940.
29 M. Barwiolek, E. Szlyk, J. Lis and T. Muziol, *Dalton Trans.*, 2011, **40**(41), 11012–11022.
30 M. Barwiolek, E. Szlyk, A. Surdykowski and A. Wojtczak, *Dalton Trans.*, 2013, **42**, 11476–11487.
31 *CrysAlis RED and CrysAlis CCD*. Oxford Diffraction Ltd., Abingdon, Oxfordshire, England, 2000.
32 G. M. Sheldrick, *Acta Crystallogr., Sect. A: Fundam. Crystallogr.*, 2008, **64**, 112.
33 A. L. Spek, Platon package, *Acta Crystallogr., Sect. D: Biol. Crystallogr.*, 2009, **65**, 148–155.
34 K. Brandenburg, *DIAMOND, Release 2.1e*. Crystal Impact GbR, Bonn, Germany, 2001.
35 L. J. Farrugia, *J. Appl. Crystallogr.*, 1997, **30**, 565.
36 H. Günther, *NMR Spectroscopy, Basic Principles, Concepts, and Applications in Chemistry*, Wiley & Sons, 1995.
37 M. Gullotti, A. Pasini, P. Fantucci, R. Ugo and R. D. Gillard, *Gazz. Chim. Ital.*, 1972, **102**, 855–892.
38 R. C. Felicio, G. A. da Silva, L. F. Ceridorio and E. R. Dokal, *Synth. React. Met. Org. Chem.*, 1999, **29**(2), 171–192.
39 H. E. Smith, J. R. Neergaard, E. P. Burrows and F.-M. Chen, *J. Am. Chem. Soc.*, 1974, **96**(9), 2908–2916.
40 A. B. P. Lever, *Inorganic Electronic Spectroscopy*, Wiley-Interscience, Hoboken, NJ, 2006.
41 M. Shakir, M. Azam, Y. Azim, S. Parveen and A. U. Khan, *Polyhedron*, 2007, **26**, 5513–5518.
42 W. Schlif, B. Kamieński and T. Dziembowska, *J. Mol. Struct.*, 2002, **602–603**, 41–47.
43 P. T. Kaye and K. W. Wellington, *Synth. Commun.*, 2001, **31**(16), 2405–2411.
44 J. A. Connor and R. J. Kennedy, *J. Chem. Soc., Perkin Trans. 2*, 1990, 203–207.
45 C. Maxim, F. Tuna, A. M. Madalan, N. Avarvari and M. Andruh, *Cryst. Growth Des.*, 2012, **12**, 1654–1665.
46 Ch. M. Wansapura, Ch. Juyoung, J. L. Simpson, D. Szymanski, G. R. Eaton, S. S. Eaton and S. Fox, *J. Coord. Chem.*, 2003, **56**, 975–993.
47 G. Plesch, C. Friebel, O. Švajlenová and J. Krätsmár-Šmogrovič, *Polyhedron*, 1995, **14**, 1185–1193.
48 G. Plesch, C. Friebel, S. A. Warda, J. Sivy and O. Švajlenová, *Transition Met. Chem.*, 1997, **22**, 433–440.
49 J. Jezierska, A. Jezierski, B. Jezowska-Trzebiatowska and A. Ozarowski, *Inorg. Chim. Acta*, 1983, **68**, 7–13.
50 M. Leluk, B. Jezowska-Trzebiatowska and J. Jezierska, *Polyhedron*, 1991, **10**, 1653–1656.
51 M. Asadi, B. Hemmateenejad and M. Mohammadikish, *J. Coord. Chem.*, 2010, **63**, 124–135.
52 P. Zabierowski, J. Szklarzewicz, K. Kurpiewska and K. Lewiński, *Polyhedron*, 2013, **49**, 74–83.
53 K. Nakamoto, *Infrared and Raman Spectra of Inorganic and Coordination Compounds*, Wiley, New York, 2009.
54 P. Gluvchinsky and G. M. Mockler, *Spectrochim. Acta, Part A*, 1997, **33**, 1073–1077.
55 E. Hadjoudis, A. Rontoyianni, K. Ambroziak, T. Dziembowska and I. M. Mavridis, *J. Photochem. Photobiol., A*, 2004, **162**, 521–530.
56 A. Mukherjee, A. Dutta, A. D. Jana and G. K. Patra, *Inorg. Chim. Acta*, 2013, **404**, 131–143.